Chapter 8

Segregation of P in Sub-Rapid Solidified Steels

Na Li, Shuang Zhang, Jun Qiao, Lulu Zhai, Qian Xu, Junwei Zhang, Shengli Li, Zhenyu Liu, Xianghua Liu and Guodong Wang

Additional information is available at the end of the chapter

http://dx.doi.org/10.5772/50564

1. Introduction

Macro-segregations of different kinds and degrees exist not only in traditional continuous-cast thick blanks, but also in continuous-cast thin slabs and even thinner cast strips, even though the solidification speed has increased significantly. Atom of P is center segregated in continuous-casting blanks and slabs, while center negative segregation of P is found in strip cast samples. The macro-segregation of P is also recently found in rapidly-solidified steel droplets. The macro-segregation can not be removed during the following rolling and heat treatment and has negative impacts on product properties; therefore, it is one of the most important research subjects of steel.

There is an increasing need to create high-quality steels from steel scraps due to economic and ecological reasons. Phosphorus is one of the most notorious impurities in steel scraps, which can result in steel embrittlement. On the other hand, P is beneficial in providing a fine solidification structure by decreasing the prior-γ grain size in the cast steels, and can improve the properties such as strength and corrosion resistance as long as it is in solid solution. Therefore, if P remains finely dispersed, it is possible to overcome the poor properties to some extent, even in low grade steels [1].The weathering steels with P addition have been demonstrated to have a better corrosion resistance than carbon steels in various atmospheres [2,3]. Yoshida et al.[4,5] reported the beneficial effects of P addition on prior austenite grain refinement in low carbon steels containing high content of impurity and cooled at the cooling rates from 0.1 to 40 K s^{-1}.

2. Segregation of P in Twin-Roll Casting Strips

Near-net-shape-casting processes with high cooling rates are thought to be appropriate for forming ultra-fine grained steels from steel scraps [6]. Strip casting technique is a process to produce strip coils directly from molten steel with the conventional hot rolling process being omitted, which is a potential substitute to hot strip rolling. The progress in strip-casting technology with low production cost [7] makes it possible to increase the cooling rate and resist the equilibrium segregation of alloying elements during casting.

In the present study, low carbon steel strips with different P addition were produced using the twin roll strip casting process and the effects of P on microstructure were studied.

2.1. Experimental

Low carbon steels with different P contents were prepared by melting in a 10 kg-medium-frequency induction furnace. Steel strips with 240 mm in width and 1.2 mm in thickness were produced using a vertical type twin roll strip caster followed by air cooling.

Figure 1 shows the schematic diagram of the twin roll strip caster.

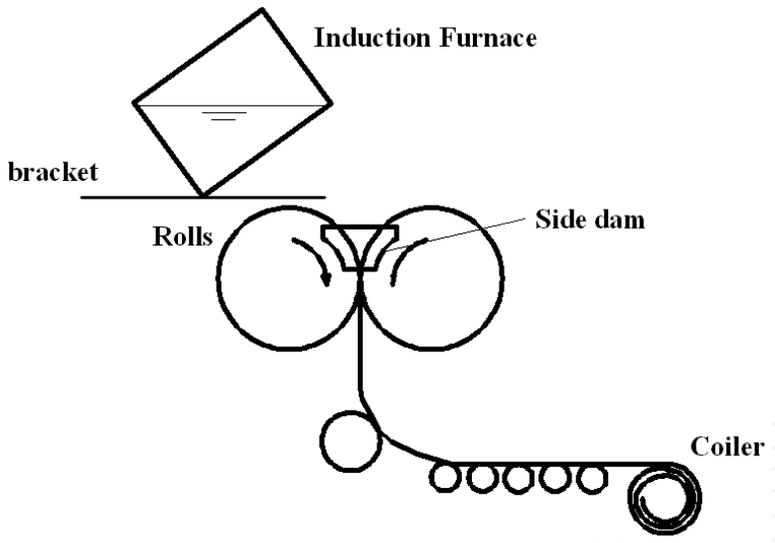

Figure 1. Schematic drawing of the operating lab-scale strip caster.

The experimental steels had a base composition of 0.16C-0.15Si-0.60Mn in mass fraction, and P content varied from 0.008% to 0.70% in weight percent. The chemical compositions of the test steels are listed in Table 1. For comparison, a sample designed as Z01 with the same composition as P01 was cast with the normal mould followed by air cooling. Samples were cut from the as-cast strip along the casting direction after casting, followed by polishing and etching with a reagent of nital at room temperature. The samples were examined using an optical microscope (OM), a scanning electron microscope (SEM) and X-ray diffraction (XRD) analysis.

Heat number	C	Mn	Si	P	Cu	Al	S
P00	0.160	0.623	0.133	0.008	0.003	0.007	0.004
P01Z01	0.158	0.607	0.140	0.100	0.301	0.009	0.006
P03	0.160	0.599	0.157	0.280	0.300	0.004	0.004
P05	0.156	0.630	0.143	0.520	0.312	0.009	0.011
P07	0.162	0.605	0.130	0.680	0.300	0.006	0.007

Table 1. Chemical compositions of test steels wt %.

2.2. Microstructure

XRD results of the as cast strips show that all the samples composed of α-ferrite and pearlite, which corresponds to the peaks of cementite in the XRD spectrum. However, XRD analysis gives less information about the amount of each phase. Figure 2 shows the microstructural observations on the cross section along the rolling direction. More α-ferrite precipitated near the surface of the samples with higher P content.

Quantitative micrographic tests were performed to decide the volume fraction of α-ferrite near the samples surfaces, as shown in Figure 3. By adding 0.68% phosphorus, there is about 90% α-ferrite precipitates in the steel. The morphology of α-ferrite transformed from widmanstaten ferrite to globular ferrite when P content was more than 0.3%. This may relate to the finer grains, which lead to the shorter diffusion distances of carbon and iron atoms.

Figure 2 also shows that the as-cast microstructures by twin-roll casting are finer than those of normal casting. Finer grains were achieved with the increase of the P content. Figure 4 shows the SEM microstructures of the cast strips. It can be seen that pearlite and bainite developed near the surfaces of the samples. The prior-γ grain size, *dr*, was also evaluated using Eq. (1) [8,9]:

$$dr = \left(A_g / n\right)^{0.5} \tag{1}$$

where A_g is the observed area and n is the number of prior-γ grains in this area. Film-like α-grains were observed along the prior-γ grain boundaries in the etched microstructure, and were used as markers for the prior-γ grain boundaries. The measured and calculated results are shown in Figure 5. The grain size decreased remarkably with P content increasing from 0.008% to 0.03%, while the decrease gradient become lower when the P content is higher than 0.3%.

Prior γ grains precipitated mainly near the surface of the strips, and there were less γ grains in the central regions. More γ grains precipitated in the surface region where reaches the austenitizing temperature more quickly and consequently offers more growing time than the center during the strip casting process. Calculation results indicated [10] that the surface region suffers a reheating process when the strip leaves the rolls, causing further growth of the γ grains.

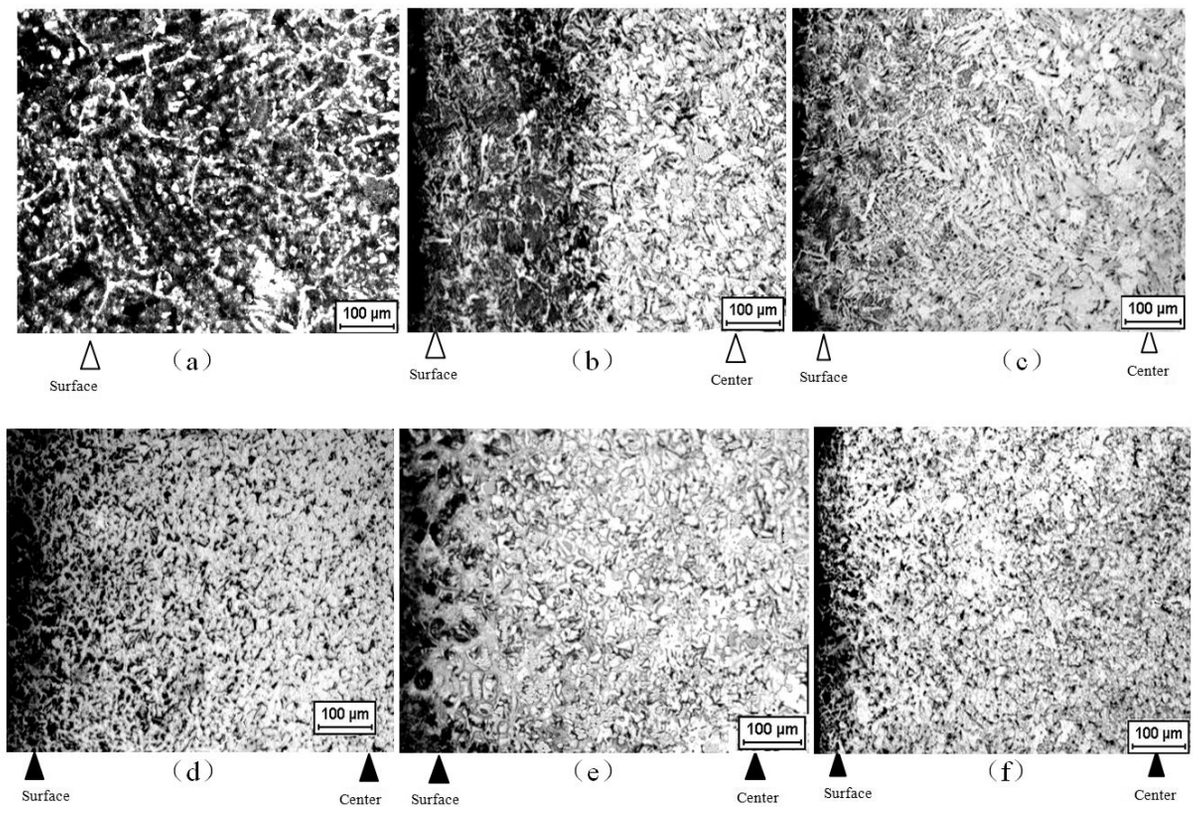

Figure 2. The microstructure of each sample: (a) Z01, (b) P00, (c) P01, (d)for P03, (e) P05 and (f) P07.

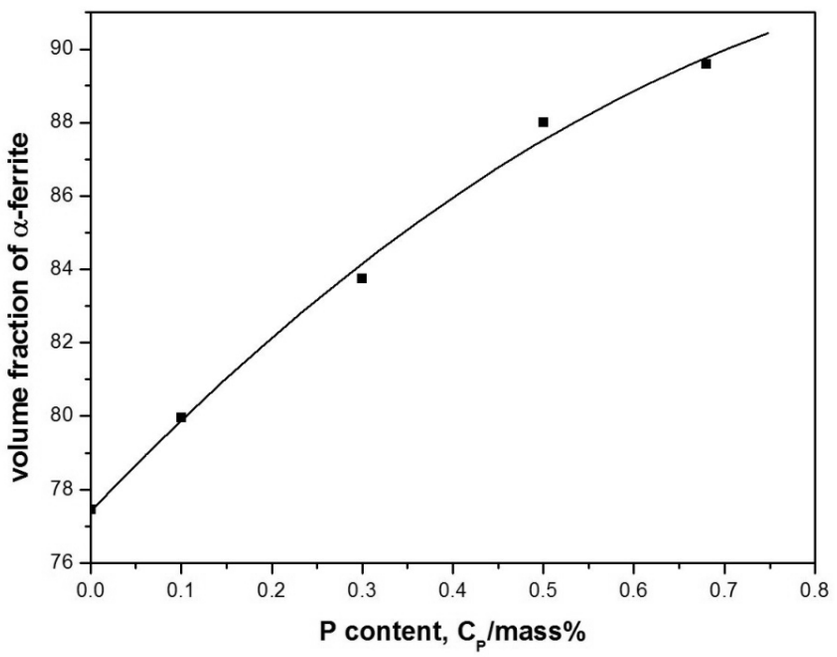

Figure 3. The volume fraction of αferrite phase with different phosphorus addition.

http://dx.doi.org/10.5772/50564

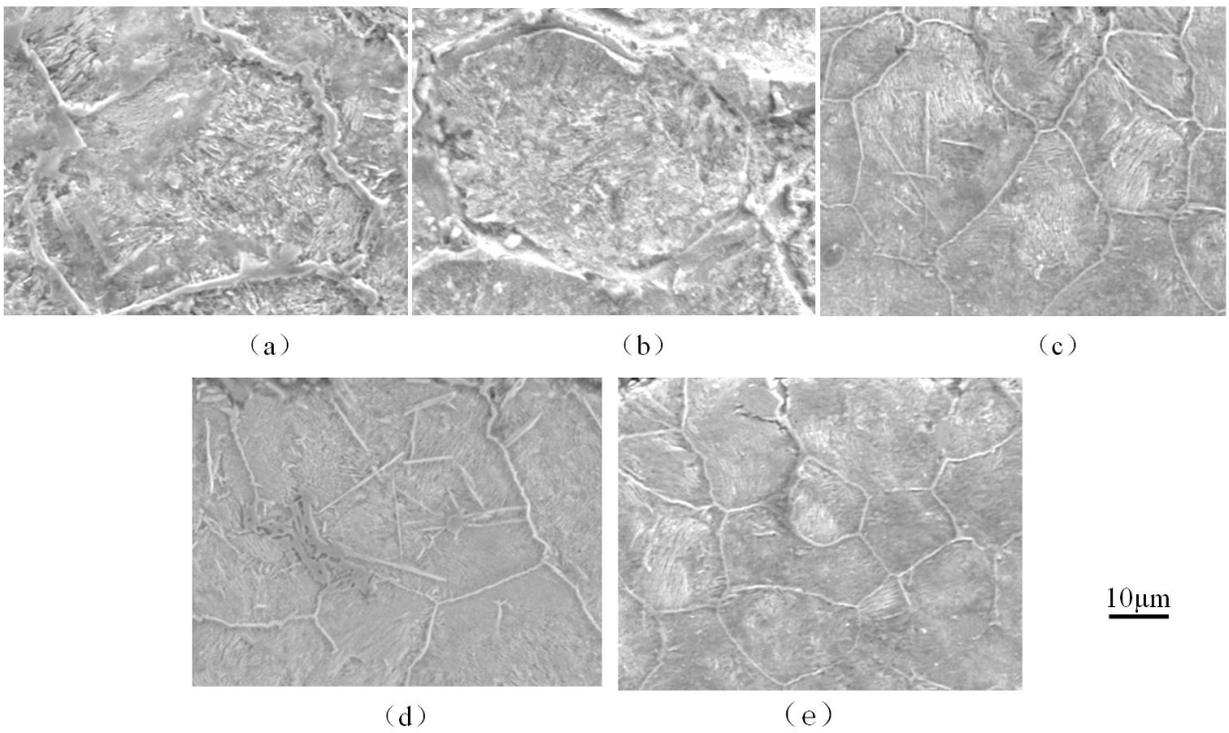

Figure 4. Microstructure near the surface of as-cast strip in the longitudinal section of (a) P00 (b) P01 (c) P03 (d) P05 and (e) P07.

2.3. P Distribution

Figure 6 shows the P distribution examined by EPMA through the whole cross-section of sample P01 and P03, P05 and P07. With P content below 0.1%, no obvious macro-segregation behavior was detected, P distributed uniformly through the thickness section. While in the steels with P content of more than around 0.3%, more P distributed near the surfaces than that at the center. The peak values may correspond to phosphide eutectics or P micro-segregation.

Fig. 7 shows the scanning maps and EDX results of P near the surface of P01 and P03. In P00 and P01, no obvious P segregation region was found by EPMA. While small phosphide eutectics can be found in sample P03, P05 and P07. Most eutectics prefer to form near the strip surfaces at the grain boundaries. This kind of phosphide eutectics must precipitate during solidification process, that is, the liquid-solid phase transformation process. While the small round phosphide showed in Fig. 8 may precipitate during the solid-solid phase transformation, and the P content in these phosphide is a little lower than that in phosphide eutectics. And the P content in the grain was also much higher than the normal value, indicating that there was much P acting as solid solution in the high-P samples.

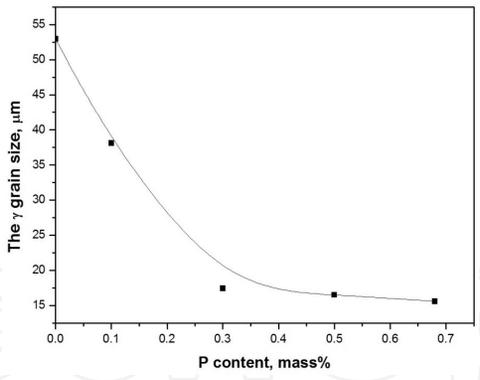

Figure 5. Effect of P content on the γ grain size.

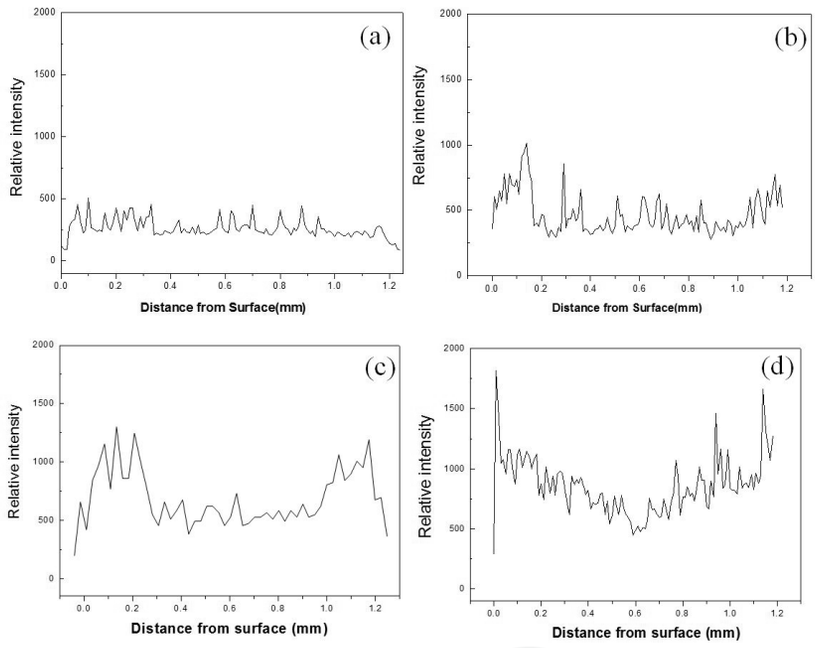

Figure 6. EMPT test results of P of sample P01(a), P03(b), P05(c), P07(d) along the thickness direction.

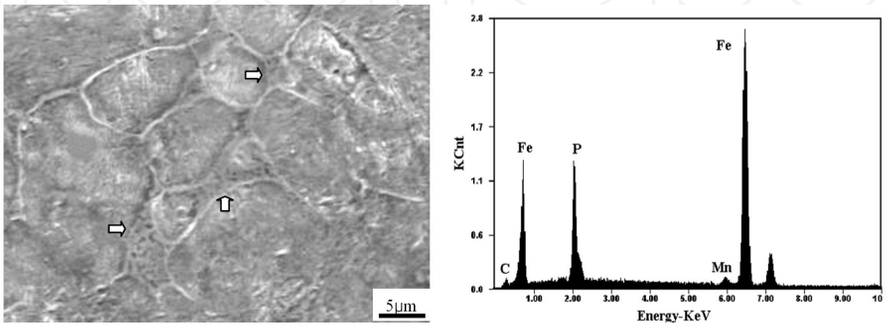

Figure 7. The morphology of phosphide eutectics and corresponding EDX in sample P03.

http://dx.doi.org/10.5772/50564

After the samples were annealed (at 1073K for 1h) and cooled rolled (to 0.65mm), the P distribution along the cross section of the samples also showed the same tendency as the cast samples (Fig. 9), which indicated that P distributions can be maintained until its usage stage of the steel.

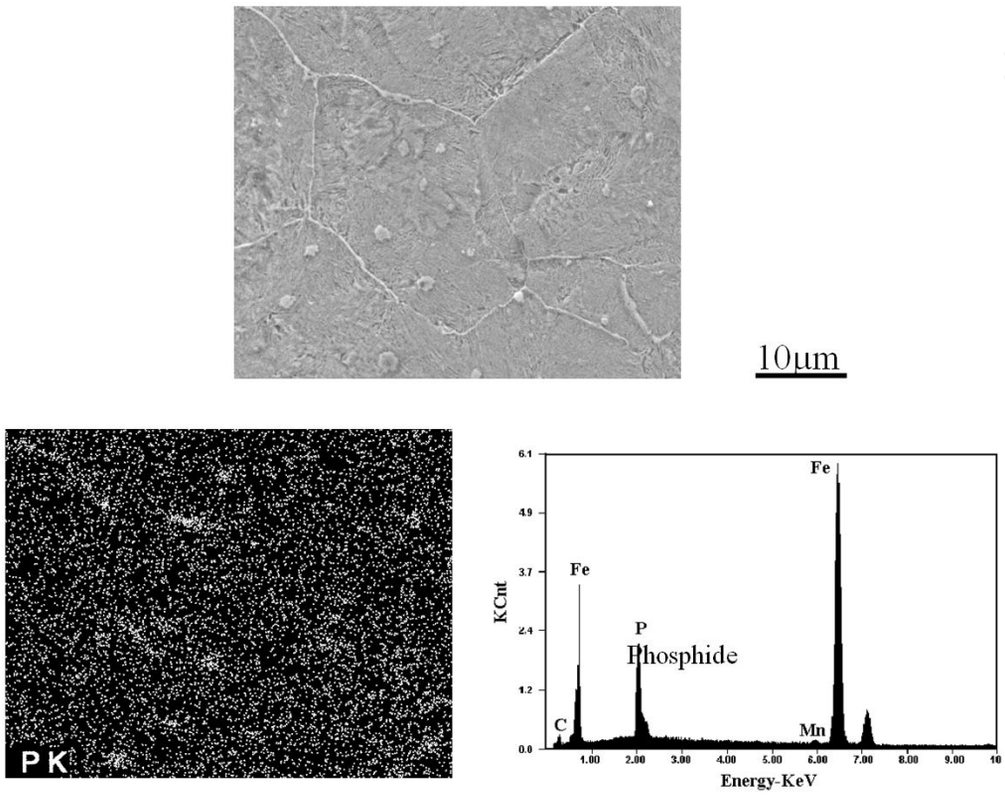

Figure 8. The mapping images of phosphorus micro-segregation in P03 by EDX.

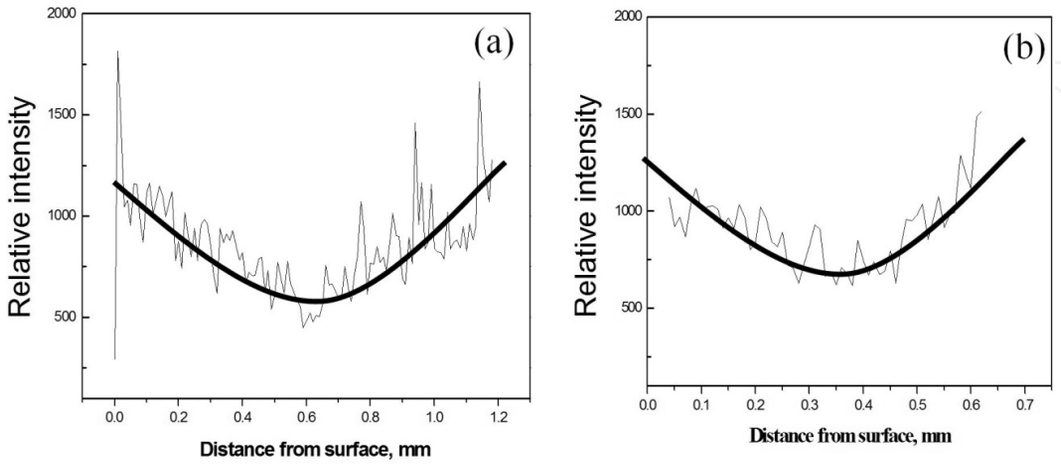

Figure 9. P distribution profiles along the thickness direction of 0.7P before (a) and after (b) annealing and cold rolling.

2.4. Properties

Micro-hardness

Test points distributed uniformly from one surface to another through the cross-section of the samples, and all test showed centro-symmetrical results. Fig. 10 shows the micro-hardness tests results from surface to center of each sample. The micro-hardness is higher near the surface than that at the center for all the samples, which corresponds to the distribution of α and γ phases in as-cast microstructure.

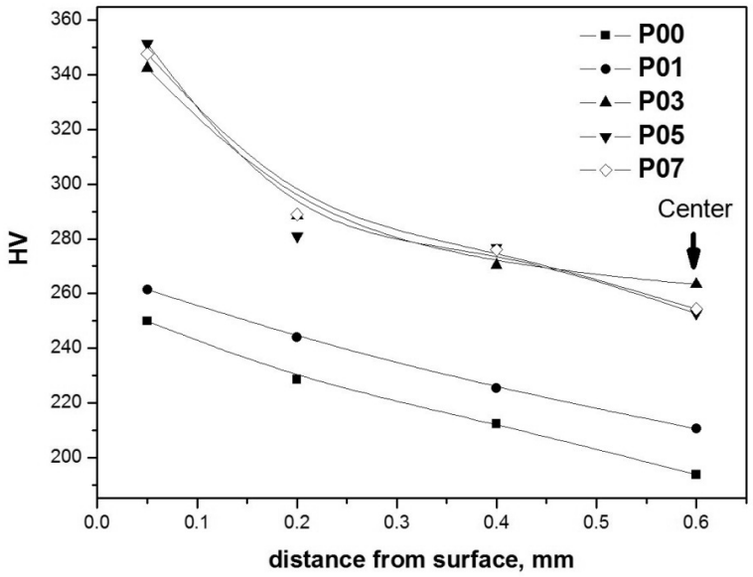

Figure 10. Micro-hardness from surface to center of each sample with different phosphorus addition.

The micro-hardness of the samples keeps increasing with the increase of P content from 0.008% to 0.68%. It is well known that P is a strong solid solution strengthening element, and the statistical micro-hardness test results also prove that most of the P atoms exist in the solid solution state in steels. The micro-hardness of P01 increased uniformly due to the well-distributed P atoms. While for sample P03, the micro-hardness near the surface is ultra high, and the relative gradient of the total curve is higher than those of the two samples with less P addition, which corresponds to the P distribution characteristic in P03 detected by EMPA. Therefore, P is an effective solution strengthening element within the studied content range and under the applied experimental conditions.

Tensile property

Tensile tests were conducted on the annealed and cold rolled samples and the results are shown in Fig. 11. The high-phosphorus steels present higher tensile strength and lower plasticity. Therefore P addition does improve the strength of the cast strips with a sacrifice of plasticity. Samples with a proper amount of about 0.01% P addition offer both high strength and elongation.

http://dx.doi.org/10.5772/50564

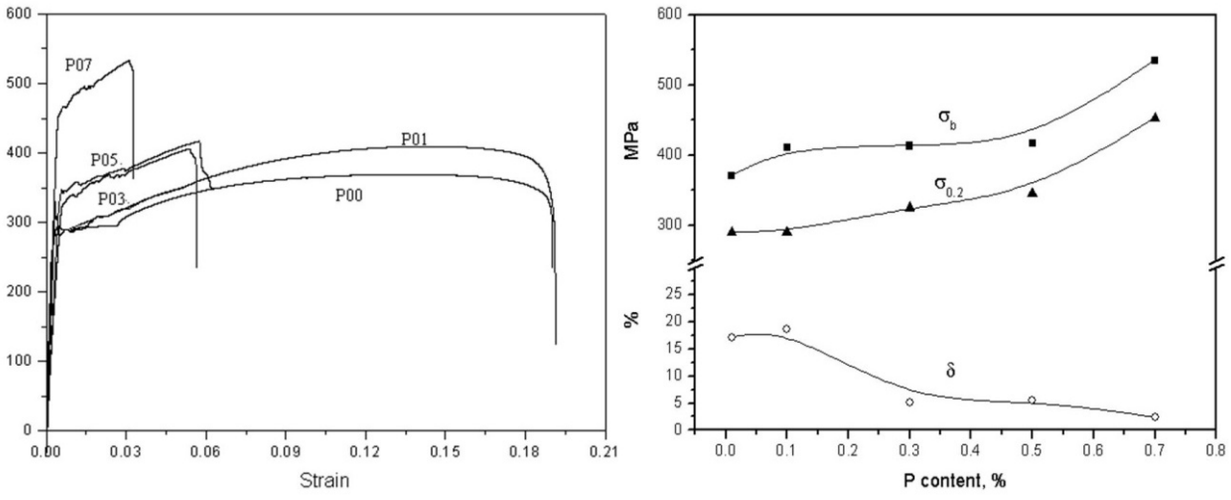

Figure 11. Tensile properties of rolled and annealed steels with different phosphorus addition.

Corrosion property

The corrosion experiments were conducted for 60 cycles with a 0.5%NaCl corrodent to simulate the see atmosphere condition. The weight increase status is shown in Fig. 12.

As shown in Fig 12, the samples with P addition exhibited high corrosion rate during the initial period, followed by rapid leveling off within 2 corrosion cycles, while the sample P00 exhibited a relatively stable corrosion rate throughout the whole corrosion process.

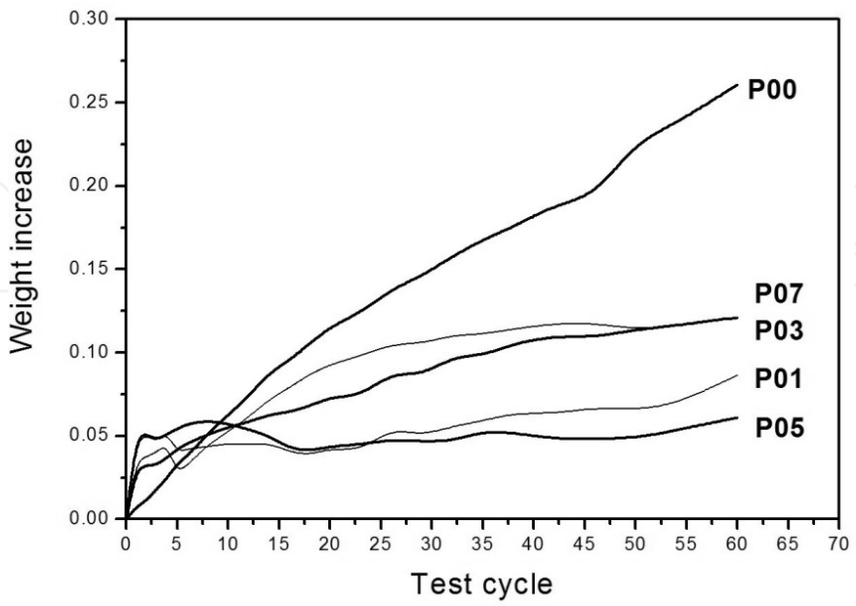

Figure 12. Corrosion properties of strip cast steels with different phosphorus addition.

The samples P01, P03, P05 and P07 show the similar corrosion properties, which indicates that P content of about 0.1% is able to increase the corrosion resistance of steel, and extra P addition can not further improve corrosion resistance.

2.5. Discussion

Phase diagram

The binary alloy containing Fe and a bcc-stabilizing element has a closed γ single phase region, or the γ-loop, in the Fe-rich side of the phase diagram [11]. Alloying elements such as P and Si can narrow the γ single phase region by decreasing the A_{e4} (δ/γ) transformation temperature and increasing the A_{e3} (γ/α) transformation temperature.

Phosphorus is a well known ferrite stabilizing element, which decreases the liquidus (T_L) and solidus (T_S) of steel and phosphorus also has a significant effect on A_{e4} and A_{e3} temperature. The addition of phosphorus in steel may lower T_L, T_S and A_{e4}, and raise A_{e3} by changing the gradients of K_L, K_S, k_{A4}, and k_{A3}, as shown in Table 2 [12], which are evaluated from the phase diagram [7] and the empirical relationship quoted by Leslie[13]. The values in the bracket in Table 2 were evaluated by thermo-dynamic calculation [5]. The A_{e4} and A_{e3} temperature for Fe-0.16C can be calculated to be 1736.5 K and 1128 K respectively, from the Fe-C phase diagram. With the gradients of transformation temperature per unit content listed in Table 2, the phase diagram of the Fe (0.16C-0.15Si-0.60Mn-0.30Cu)-P pseudo-binary system can be calculated, as shown in Fig. 13. This steel system has a typical γ-loop and a negative high gradient of δ/γ transformation temperature, or k_{A4}. The γ-loop closed at the P content of about 0.52 mass fractions. For the higher P content, no single γ phase region is formed, corresponding to the more α-ferrite volume fraction shown in Figure 3.

Element	Mn	Si	Cu	Al	P	S
K_L[K/mass%]	-4.9	-7.6	-4.7	-3.6	**-34.4**	-38
K_S[K/mass%]	-6.5	-20.5	/	-5	**-500**	-700
k_{A4}[K/mass%]	+12	-60 (-52)	/	-81	**-140 (-550)**	-160
k_{A3}[K/mass%]	-30	+44.7 (+77)	-20	+140 (+400)	**+700 (+340)**	/

The K_L and K_S are the gradient of liquidus (T_L) and solidus (T_S) of steels

The k_{A4} and k_{A3} are the gradient for A_{e4} (**δ/γ**) and A_{e3} (**γ/α**) respectively

Table 2. Effect of alloying elements on phase transformation temperature in Fe binary alloys.

P addition also has great effects on Fe-C phase diagram. Figure 14 shows the effect of P on the Fe-C phase diagram calculated by thermodynamic calculation. The mushy zone becomes wider with P addition, and the super-cooling degree increased correspondingly during solidification, which raises the amount of spontaneous nucleation and refines grains.

http://dx.doi.org/10.5772/50564

Figure 14 also shows that the single γ-phase region becomes smaller with an increasing P content until the tie line does not pass through the single γ-phase region at all with the P mass content of about 0.7. Therefore, γ-phase was prevented from both nucleation and growth in the high-P strips, and the finer grains can be observed in the test steels.

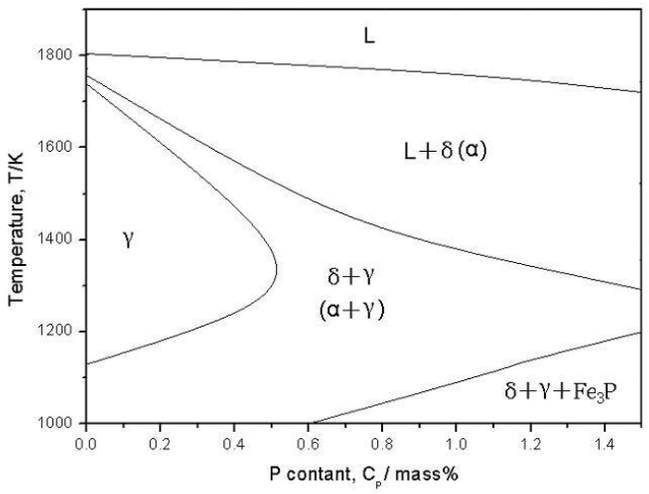

Figure 13. Phase diagram of Fe (0.16C-0.15Si-0.60Mn-0.30Cu-0.4Al-0.04S)-P pseudo-binary system.

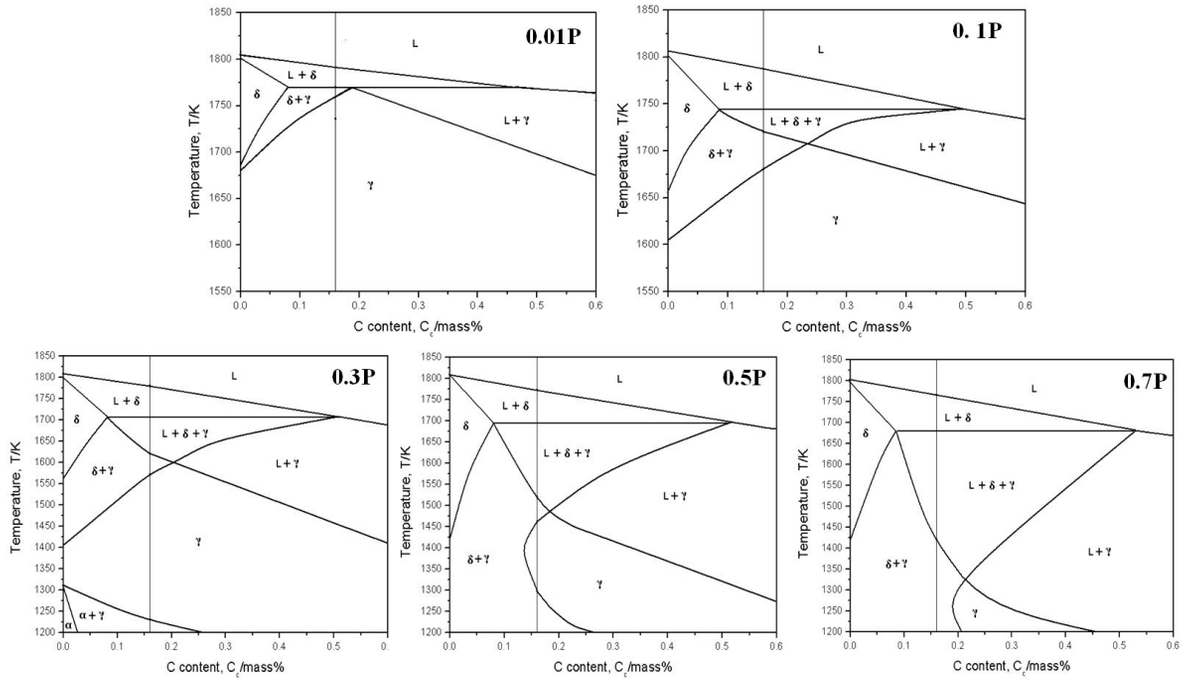

Figure 14. Phase diagrams of Fe (0.15Si-0.60Mn-0.30Cu-0.4Al-0.04S)-C pseudo-binary system with different phosphorus contents.

Solidification processing

EPMA and EDX results clearly show negative segregation at the centre of strip thickness with P content of higher than around 0.3%. Fig. 15 showed the schematic drawing of strip casting process. It is supposed that the height of liquid pool is stable during the strip cast process, and A, B and C are the schematic solidification front with different heights in the liquid pool. A solidified shell is formed near each roll surface during casting. Y.K. Shin et al [14] reported that surface inverse segregation of Mn was observed in as-cast strip resulting from the roll-separating force, and this phenomenon was not observed in the permanent mold cast strip. Y.K. Shin et al regarded [15] that as these shells were forced together and had started to be rolled, the solute enriched liquid was squeezed upwards away from the final solidification position and was extruded into prior inter-dendritic spaces, and therefore the solute content at the strip centre is consequently depleted.

However, the squeezing stress is rather low before the solidified strip is rolled, and the surfaces of the strip contract greatly at the higher cooling speed, so it is difficult for the solute enriched liquid to reach the surfaces of the strips. Meanwhile, columnar grains are significantly damaged when the solidified shell is rolled [15], and there is no obviously columnar crystals observed in the strip cast microstructures as shown in Fig. 2 and Fig. 4, there is actually no solute transmission path. Therefore, the phenomenon of high solute content near the strip surface can not be explained.

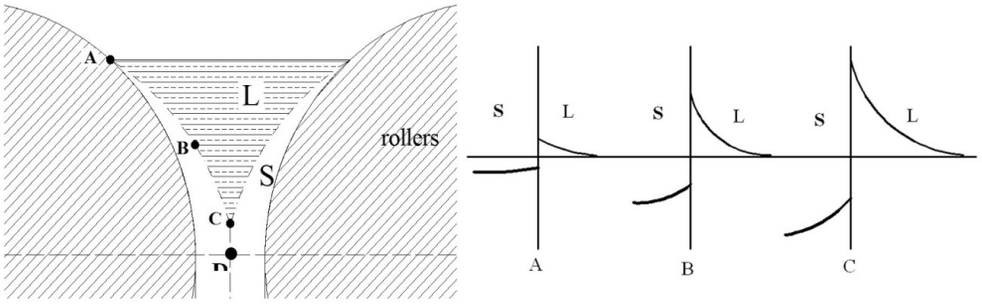

Figure 15. Schematic drawing of strip casting process.

During the strip casting process, the cooling rate near the surface is higher than that at the center of the strip, which may cause the higher partition coefficient content, that is, $K_A > K_B > K_C$ as shown in Fig. 15, and the solid solution content of P is also higher than that at the center when the P content is high enough. The coefficient K may approaches 1 when the cooling rate is high enough, implying that the solute content in solid approaches that in liquid at the solidification front.

P-rich liquid is enriched in the lower temperature regions in the melting pool [16]. Thermodynamic calculation and numerical simulation results [17] show that the lower temperature region is near the meniscus, as shown in Fig. 16. The letters A to I in Fig. 16(b) refer to the regions with corresponding temperature centigrade in the melting pool. During the strip casting process, P is redistributed in the melting pool under the stress of liquid flow and

squeezing of the rolls, and more P-rich melt prefer to distributed near the meniscus, which can enter the solidified skull under the rapid solidification condition and lead to the higher solute content at solidification front, and finally form the higher content of P near the surfaces than at the centre of the strip.

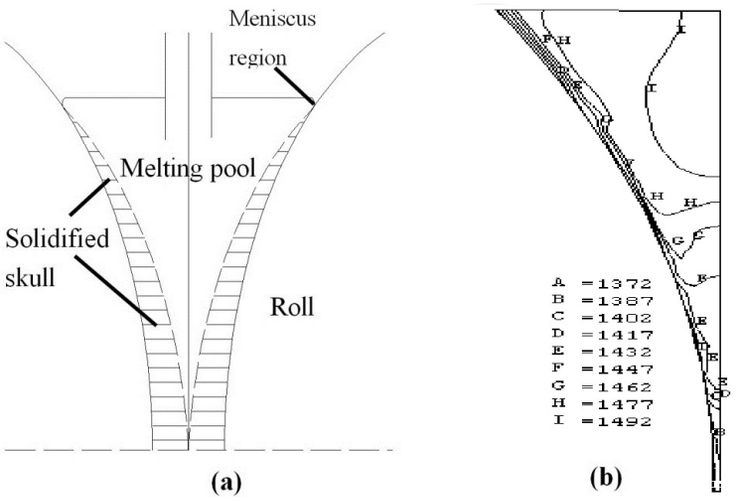

Figure 16. Schematic drawing of melting pool, (a); and typical simulated temperature fields, (b), in the middle cross section along the axial direction [18].

2.6. Effect of C on the Distribution of P

Carbon is one of the important elements in steel, and experiments also show that carbon has great affection on the segregation behavior of phosphorus [18].Carbon steels with different P and C contents were prepared using the twin roll strip caster followed by air cooling with 240 mm in width and 1.2mm, 1.4mm, and 1.8mm, in thickness, respectively.

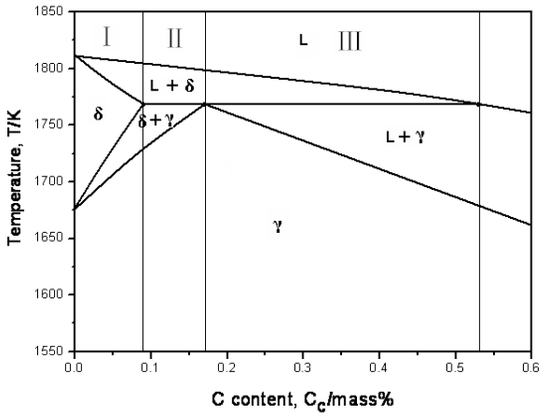

Figure 17. Part of the Fe-C phase diagram.

A portion of the Fe-C phase diagram can be divided into three parts (regions I, II, and III) at points M, N, and O as shown in Fig. 17. Three kinds of carbon steels with different carbon contents were selected in regions I, II, and III, which were designated as group I, II, and III, respectively, then different amounts of P were added by introducing the Fe-P alloy. The chemical compositions of the steels were examined and the results are shown in Table 3.

Fine grains and dendrite structure were observed in high-P steels. The distribution of P was measured by electron probe micro-analyzer (EPMA-810Q). For the steels with different carbon contents, phosphorus distribution in the thickness direction of the strip is obviously different, as shown in Fig. 18.

Group	Heat number	C	Mn	Si	P	Cu	S
I	603	**0.054**	0.121	0.334	**0.320**	0.520	0.005
	602	**0.045**	0.130	0.330	**0.600**	0.312	0.010
II	303	**0.160**	0.599	0.157	**0.280**	0.300	0.004
	307	**0.162**	0.605	0.130	**0.680**	0.300	0.006
III	206	**0.430**	0.610	0.125	**0.280**	0.300	0.011
	212	**0.440**	0.630	0.140	**0.630**	0.306	0.007

Table 3. Chemical composition of test steels wt%.

The samples taken from the head, the middle, and the end of each strip show the same results. P distribution in the thickness direction varies with different C and P contents.

It can be deduced from Fig. 17 that the higher the carbon content, the longer the length of the mushy zone (LMZ), that is, LMZI<LMZII<LMZIII. P negative segregation increases severely with increasing LMZ according to the experimental results as shown in Fig. 18.

For samples 603 and 602 of group I, the mushy zone is relatively short even though it becomes longer with more P addition [6] and it induces no obvious P segregation along the thickness direction as shown in Fig. 18. When the P content is high enough, there is a tendency of center segregation of P. The mushy zone is the longest in region III, there is obvious P negative center segregation in both strips 206 and 212. The P content near the surfaces of the strips is much higher than that near the center where the P content is relatively uniform. The negative segregation becomes severe with more P addition.

From Fig. 18, it can be observed that the segregation mode is different with different group, which may be related to the solidification outgrowth. The solidification outgrowths are δ-Fe, δ and γ phases, and single γ phase corresponding to Fig. 17, respectively. The Fe-P phase diagram shows that up to 2.8wt% P is soluble in δ(α) ferrite at 1050°C and about 1wt% P is still soluble at room temperature. Therefore, P as a trace element acts as solute in δ (α) ferrite. The solubility of P in γ phase is very low and the maximum solubility at 1200°C is only about 0.28wt%, and even lower P is soluble in γ phase at the temperature below 911°C. The solubility of P in the α+γ region is between that of the above two regions and is much lower than that in ferrite [19].

http://dx.doi.org/10.5772/50564

The α (δ) ferrite percentage in the solidification microstructure of samples 603 and 602 is very high because of the low carbon content. The solubility of P in α (δ) ferrite is higher than the content of P added in the experimental steels, and the diffusion speed of P in α-ferrite is much higher at high temperatures, so the distribution of P is rather uniform in the thickness direction of the cast strip as shown in Fig. 18.

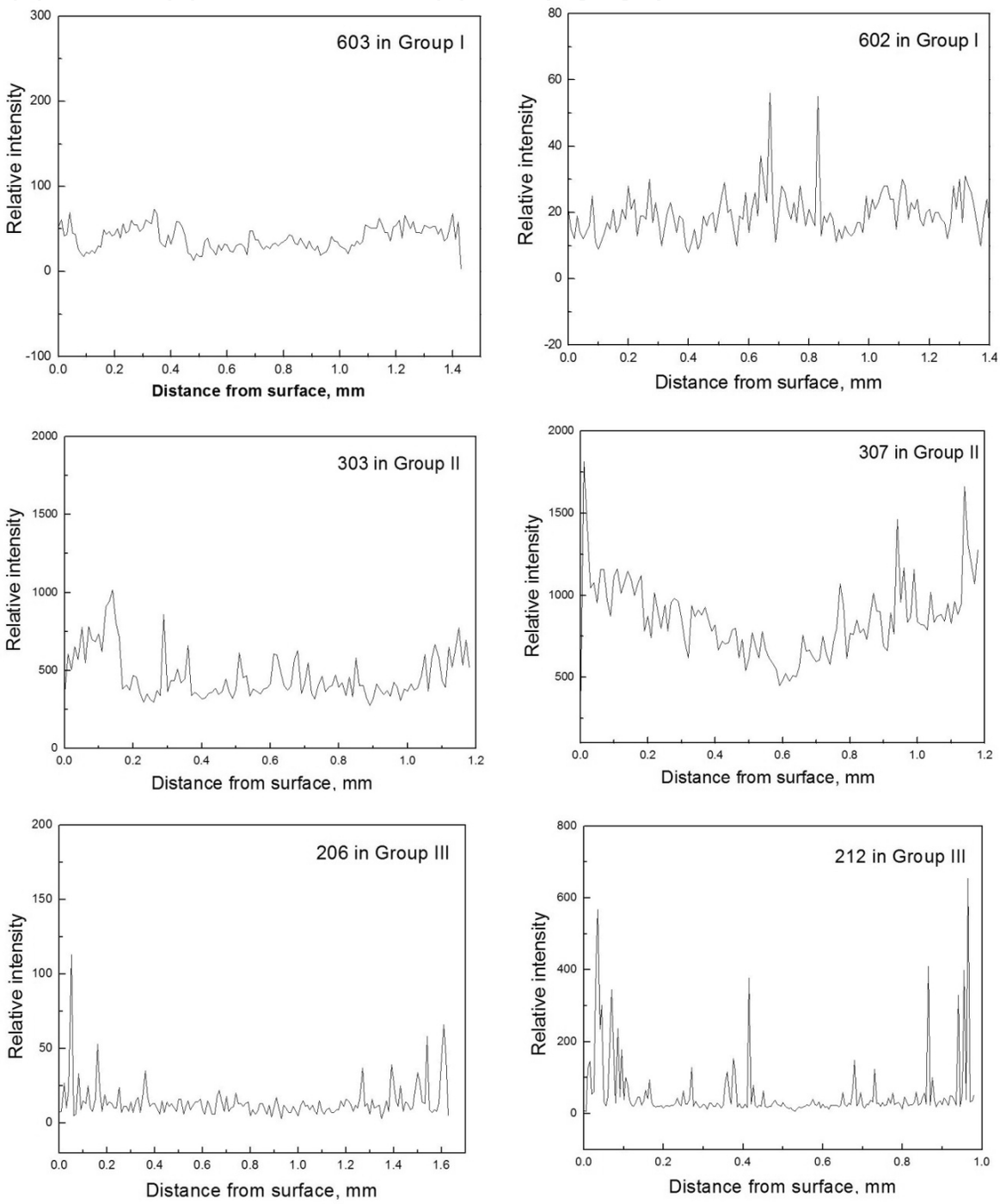

Figure 18. P distribution profiles along the cross section of each sample in different groups.

P in cast strips 206 and 212 is concentrated near the surface as shown in Fig. 18 because the solubility of P in γ austenite phase is rather low and the solidification outgrowth is only γ austenite in region III. In region II, the solidification outgrowth is α+γ and the solubility of P in α+γ is between that in α and in γ, therefore the P distribution characterization in this region is intermediate as shown in Fig. 18.

3. Segregation of P in steel droplets

Rapid solidification is a significant research subject in the field of material science and condensed physics and plays a major role in material engineering and crystal growth [20], which can remarkably increase the solid solution of alloying elements, produce fine microstructures and reduce or eliminate the segregation of alloying elements. However, the segregation of P and C was observed in rapid solidified strip-casting steel strips.

Container-less processing is an important method to realize the under-cooling and rapid solidification of materials. During container-less processing, the contact between the melt and container wall can be avoided and heterogeneous nucleation can be suppressed to some extent; hence high under-cooling and rapid solidification can be achieved. A drop tube is a special technique for investigating rapid solidification through combining high under-cooling and rapid cooling [21].

3.1. Experimental

Carbon steels with P addition and different B and C contents were prepared in a 2-kg high-frequency vacuum induction furnace, and the compositions are listed in Table 4. Small samples with the size of 2 mm × 2 mm × 2 mm (TM) and 5 mm × 5 mm × 5 mm (FM) were taken from the bulk. All the sides of the small samples were ground and then cleaned with alcohol.

The dry samples were re-melted in a suspension-type vacuum furnace and the melted droplets were then solidified in silicone oil, both the vacuum furnace and the silicone oil were placed in the vacuum drop tube. The schematic diagram of the experimental device is shown in Fig. 19. The drop heights were set to be about 0.2 m and 50m respectively.

Heat No.	C	Mn	Si	S	P	B
0	0.035	0.176	0.024	0.006	**0.005**	
1	0.035	0.179	0.036	0.004	**0.089**	--
2	0.030	0.182	0.033	0.004	**0.525**	
3	0.038	0.181	0.028	0.005	**0.097**	**0.0033**
4	**0.141**	0.178	0.033	0.004	**0.091**	

Table 4. The composition of droplet samples wt%.

http://dx.doi.org/10.5772/50564

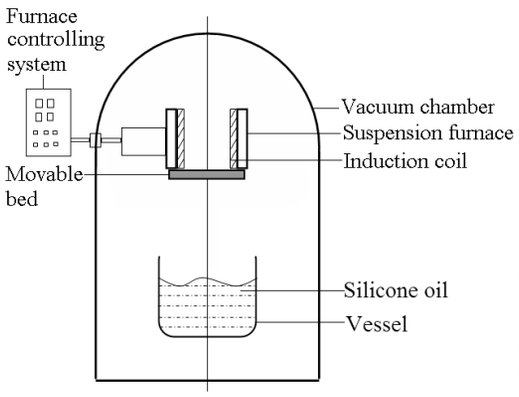

Figure 19. Schematic diagram of the vacuum drop tube.

The microstructures were observed with optical microscope, the alloying elements were detected by electron probe micro-analysis (EPMA-1610), and the micro-hardness were measured and compared with the bulk samples.

3.2. Microstructure

Microstructure at different falling height:

Fig. 20 shows the microstructure near the surface and at center of drop TM sample 1 with the falling height of 0.2m and 50m in drop tube respectively. The microstructure is fine ferrite. The convection heat transfer were ignored because of the vacuum condition in drop tube, and for the volume of the droplets were rather large, it was regarded that the solidification process happened until the liquid drops met the silicone oil even though the falling height is 50m. It can be seen from Fig. 20 that the microstructures of Fig. 20 (c), (d) were a little finer than those of Fig. 20 (a), (b). It indicated that the solidification speed was a little higher for 50m drop samples, for the decreased temperature during falling period may correspond to lower casting temperature, and the lower casting temperature can result in finer microstructure. The finer microstructures were also observed in other 50m drop samples.

By comparing Fig. 20 (a) and Fig. 20 (b), Fig. 20 (c) and Fig. 20 (d) respectively, there is not obvious difference between the microstructure near the surface and that at the center. It indicated that the solidification speed is approximately the same from the surface to the center.

Microstructure with different drop sizes:

Figures 21 and 22 show the microstructures near the surface and at the center of TM sample 1 and FM sample 1 solidified in the drop tube (all at the falling height of 0.2m). The microstructure is mainly fine ferrite. It can be seen from Figs. 21 and 22 that the microstructures in Fig. 21 are a little finer than those of Fig. 22. It may indicate that the solidification speed is a little higher for the TM drop samples. By comparing Fig. 21 (a) with Fig. 21 (b), and Fig. 22 (a) with Fig. 22 (b), it was found that there is no obvious difference between the microstructure near the surface and that at the center. It indicates that the solidification speed is approximately the same from the surface to the center for both TM and FM samples.

For sample 2 with higher carbon content, as shown in Figs. 23 and 24, the microstructures of FM sample 2 are rather finer than those of the FM sample 1 and of the TM samples 1 and 2. This is opposite to the observed results for sample 1; and the microstructures are uniform from the center to the surface. It was analyzed that, recalescence is an important phenomenon that could not be ignored during the rapid solidification process. Recalescence comes from the release of the latent heat of crystallization, which is in direct proportion to the volume of the melt. So the effect of recalescence on the FM samples is considerably greater (more than 15 times) than that on the TM samples. When the carbon content is increased in the steel, the heat transfer capability and the latent heat of crystallization are decreased gradually [22]. So the solidification speed is higher in sample 2 than that in sample 1, which leads to the finer grains. Moreover, the carbon content of sample 2 approaches the eutectoid steel, which may make the microstructure further refined during the cooling process after solidification.

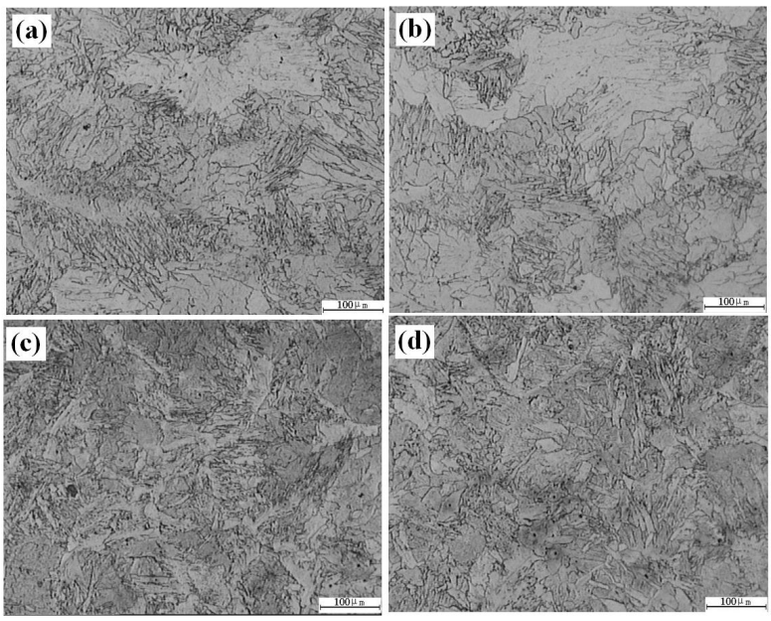

Figure 20. Microstructures of droplets TM sample 1. (a), (b) with the falling height of 0.2m: (a) near the surface, and (b) at the center; (c), (d) with the falling height of 50m: (c) near the surface, and (d) at the center.

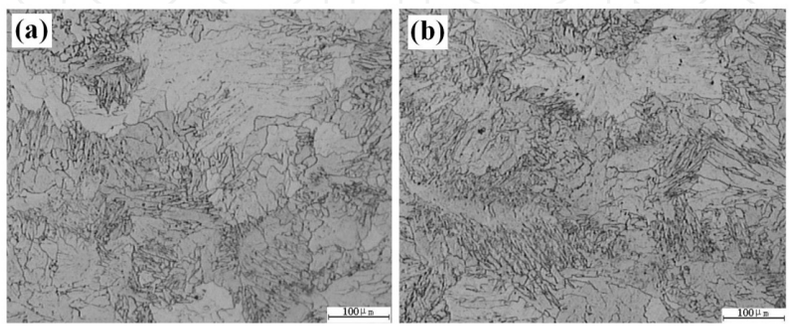

Figure 21. Microstructures of steel droplet TM sample 1: (a) at the center, (b) near the surface.

http://dx.doi.org/10.5772/50564

For sample 2 with higher carbon content, the microstructure of TM samples at the center (Fig. 23a) is quite different from that near the surface (Fig. 23b). There is more pearlite appearing near the surface. This means there is higher carbon content near the surface than at the center, where the microstructure presents more ferrite. The surface temperature of the droplet sample declines to γ phase zone earlier than the center during the solidification process, and the solidification speed near the surface reduces due to the release of latent heat of crystallization [23], even though it is not re-melted.

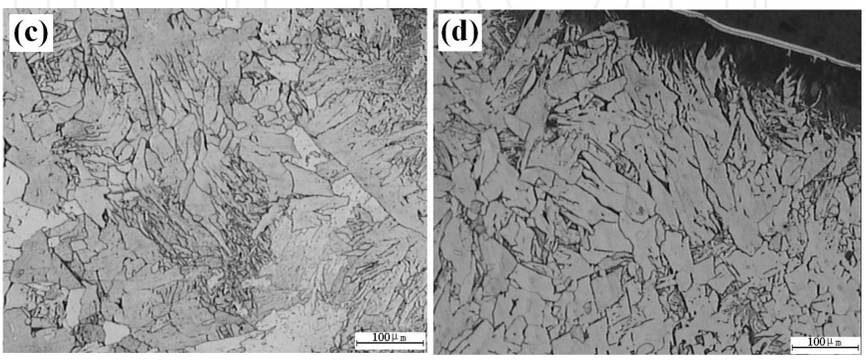

Figure 22. Microstructures of steel droplet FM sample 1: (a) at the center, (b) near the surface.

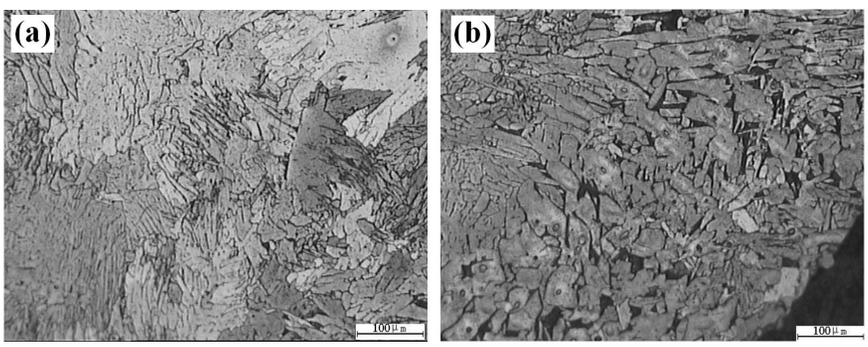

Figure 23. Microstructures of steel droplet TM sample 2: (a) at the center, (b) near the surface.

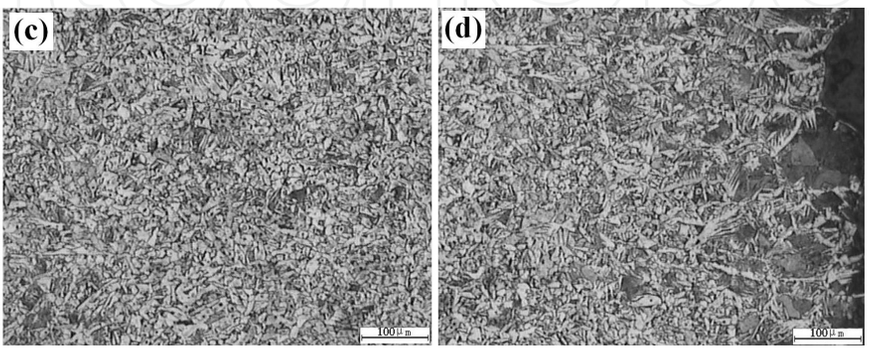

Figure 24. Microstructures of steel droplet FM sample 2: (a) at the center, (b) near the surface.

The surface is kept a relative longer time in γ phase zone than that in the center region. The carbon atoms may diffuse to the γ phase zone as the solid solution of C in the γ phase is much higher than that in the α phase. This may lead to the segregation of carbon near the surface region. For the TM sample 2, the carbon content of most local regions is far away from the eutectoid steel, and there are more ferrite at the center and more pearlite near the surface, so the microstructure is not so fine and uniform.

3.3. P distribution

The distribution of alloying elements P and C were detected along the diameter of each droplet sample. For sample 1, When the P content was less than about 0.1 mass % in low carbon steels, P did not show obvious segregation in rapid solidified droplet samples; the distribution of C also showed nearly uniformity throughout the whole sample, including both the 0.2m and 50m droplet samples.

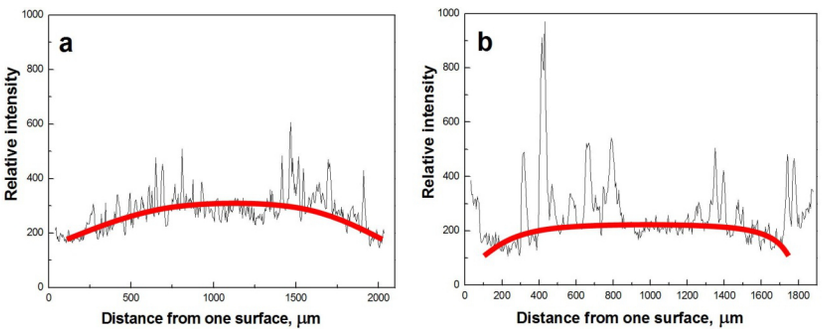

Figure 25. Distribution of P from one surface to another throughout the droplet samples 3: (a) for 0.2m droplet samples, and (b) for 50m droplet samples.

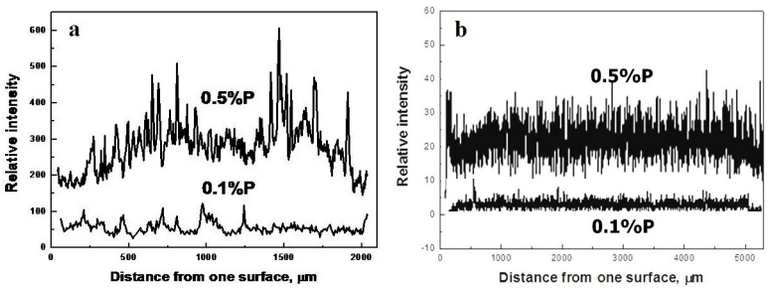

Figure 26. P distribution profiles along the diameter of droplet sample 1# (0.1%P) and 2# (0.5%P) (a, TM samples and b, FM samples).

Fig. 25 shows the distribution of P in sample 3 with higher P content. When the P content rose up to about 0.5 mass% in the samples, both 0.2m droplet samples (Fig. 25a) and 50m droplet samples (Fig. 25b) showed P center segregation and nearly uniformity C distribution. The difference in falling height did not affect the distribution of alloying elements obviously.

The segregation of P was observed in TM samples while not in FM samples, as shown in Fig. 26. This is regarded as relating to recalescence and the diffusion of C and P atoms during the solidification process [24,25].

3.4. Distribution of C with P addition

The distribution of C was detected along the diameter of each droplet sample. For sample 1, the distribution of C is nearly uniform throughout the whole sample, including both TM and FM droplet samples, as shown in Fig. 27.

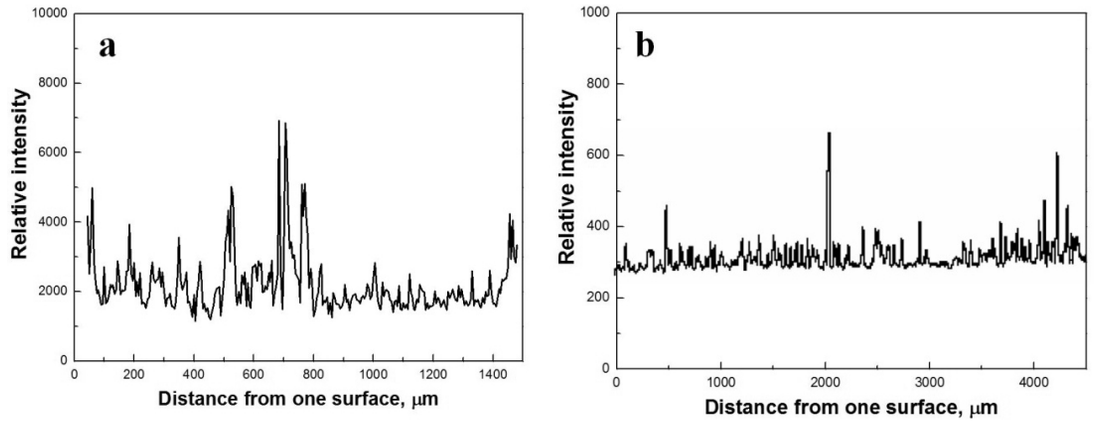

Figure 27. Distribution of C throughout the diameter of droplet TM 1 (a) and FM1 (b) samples.

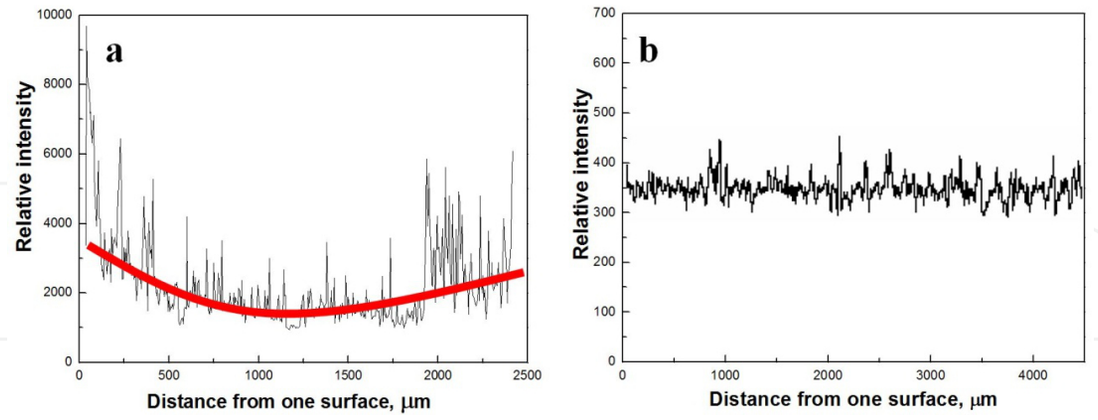

Figure 28. Distribution of C f throughout the diameter of droplet TM 2 (a) and FM 2(b) samples.

For the TM sample 1, the relatively higher C content was observed both near the surface and at the center as shown in Fig. 27 (a). The fluctuation of C distribution indicates that the small volume samples are affected greatly by the cooling and surrounding conditions, including the release of latent heat of crystallization. For the FM sample 1, the distribution of C is more uniform, as shown in Fig. 27 (b), this may relate to the greater amount of latent heat of crystallization.

With higher C content, the segregation of C was observed in TM sample 2, as shown in Fig. 28(a). The C content near the surface is higher than that at the center. The distribution of C is corresponding to the microstructure of the TM sample 2, as shown in Fig. 23, where there are more pearlites near the surface and there are more ferrite near the center.

In the FM sample 2, the uniform C distribution was observed as well, as shown in Fig. 28 (b), which also corresponds to the microstructures, as shown in Fig. 24. This may suggest that the intensity of cooling is equivalent to the latent heat of crystallization.

3.5. Effect of B on the distribution of P

The distribution of C and P were detected along the diameter of droplet sample 1 and sample 3, as shown from Fig. 29 to Fig. 32.

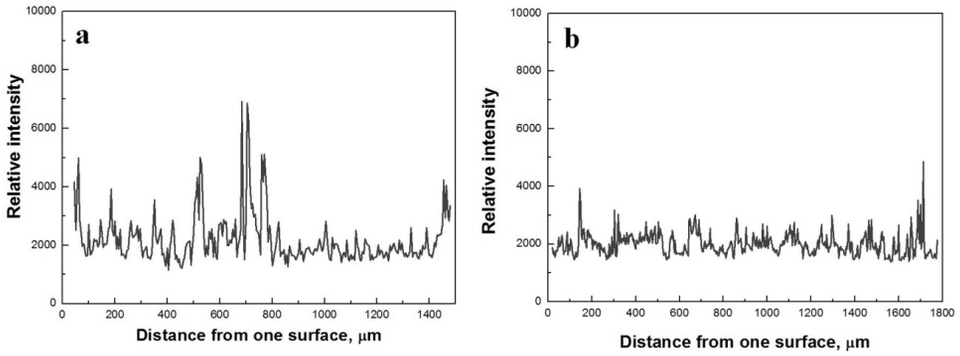

Figure 29. Distribution of C from one surface to another throughout the droplet samples TM 1 (a) and TM3 (b).

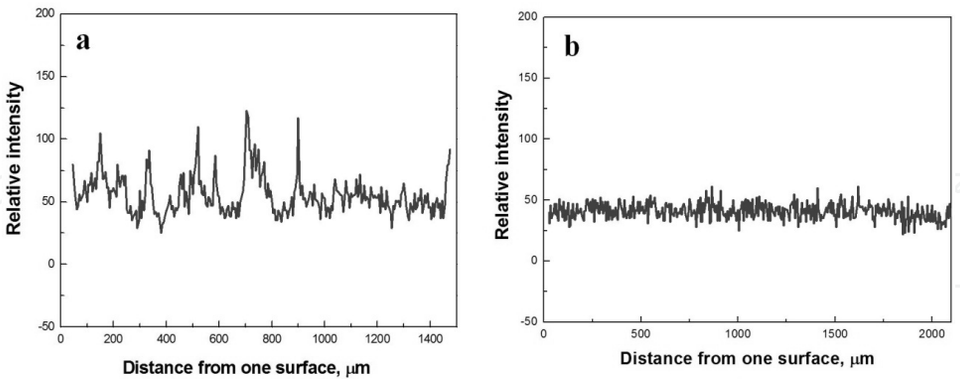

Figure 30. Distribution of P from one surface to another throughout the droplet samples TM 1 (a) and TM 3 (b).

For all the samples, the distributions of both C and P were much uniform in B-bearing samples than those in B free samples. Fig. 29 shows the C distribution profile along the diameter of the droplets TM1 (Fig. 29a) without B addition and TM 3 (Fig. 29b) with B addition, with the same relative intensity as vertical coordinate, it is obviously shows that B atoms can promote the uniformity of C in the rapid solidified steel.

http://dx.doi.org/10.5772/50564

B also can promote the uniformity distribution of other element such as P in rapid solidified steel sample, as shown in Fig. 30. The effect of B on the distribution of C and P in rapid solidified steel samples is also notable as shown in Fig. 31 and Fig. 32 when the volume of the samples increased.

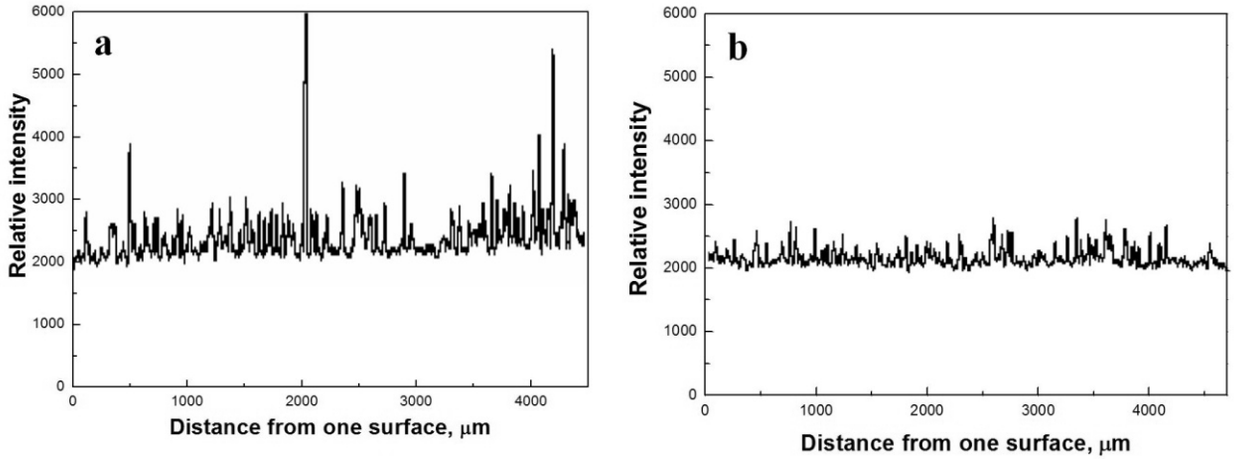

Figure 31. Distribution of C from one surface to another throughout the droplet samples FM 1 (a) and FM 3(b).

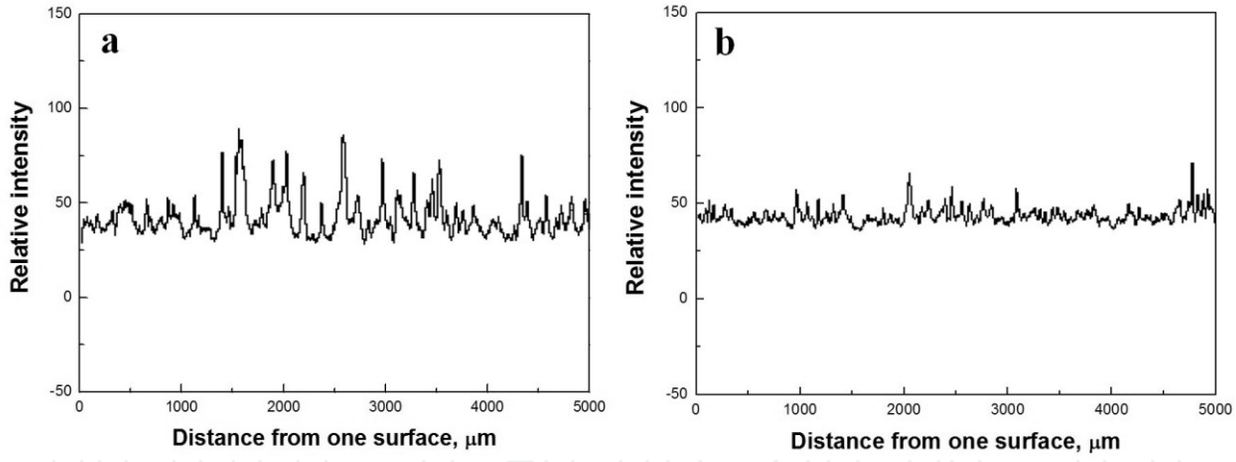

Figure 32. Distribution of P from one surface to another throughout the droplet samples FM 1 (a) and FM3 (b).

It also should be noticed that, the distribution of C and P becomes more uniformly when the volume of the samples increased by comparing that in sample TM 1 (Fig. 29a, Fig. 30a) and FM 1 (Fig. 31a, Fig. 32a) respectively. For TM samples, the volume of the samples is smaller and it is easily affected by the solidification conditions, and the latent heat of solidification increased with the larger volume of the FM samples, which present a more stable system during rapid solidification, and this may induce the more uniform distribution of alloying elements C and P. At the same time, the distribution of C and P in B-bearing FM samples (Fig. 31b, Fig. 32b) shows also more uniform than that in B free TM samples (Fig. 29b, Fig. 30b).

3.6. Micro-hardness

The micro-hardness (HV) of the original cast samples and all the TM and FM samples were measured in this experiment. For each samples, the differences between the maximum and minimum test value was within 15HV, which may be caused by the segregation of elements or the precipitation of compound phases, and the mean value was shown in Table 5. It can be seen from Table 5 that the micro-hardness of rapid solidified samples are much higher than those of original bulk samples. The micro-hardness of rapid solidified FM samples with larger volume show lower values than those of TM samples.

Sample No.	Bulk	TM	FM
0	97.93	133.85	125.96
1	118.22	157.33	150.49
2	203.13	239.01	227.36
3	135.31	184.15	159.86
4	130.72	171.95	167.41

Table 5. The micro-hardness (HV) of each sample.

Under each condition, the samples with higher P content show obviously higher micro-hardness than those with less P content, and when the C content increase, the samples show higher micro-hardness correspondingly.

The micro-hardnesses of B-bearing samples are higher than those of B-free samples, while this tendency weakened when the volume of droplet samples increased. So adding certain account of B in the steel can strengthen the material, even under the rapid solidified conditions.

4. Conclusions

(1) Finer as-cast microstructures have been obtained in twin-roll casting strips and droplet samples than those of normally cast bulk samples. The microstructures of 50m droplet samples are a little finer than those of 0.2m droplet samples. The solidification speed is approximately the same from the surface to the center of each sample.

(2) When the C content is rather low, the microstructures of the TM ($2\times2\times2mm^3$) droplet samples are a little finer than those of the FM ($5\times5\times5mm^3$) samples. When the C content increases to approach that of eutectoid steel, the microstructures of the FM samples are much finer than those of the TM samples. This may be related to the lower latent heat of crystallization when the carbon content increases. Meanwhile, the eutectoid steel and the microstructures may be refined during the cooling process after solidification.

http://dx.doi.org/10.5772/50564

(3) Much finer grains are observed with increasing P content, while the grain size decrease slightly when the P content is higher than 0.3% in mass. There are more α-ferrites precipitated with the increase of P content and the α-ferrites become globular. More α-ferrites present at the centre.

(4) In samples with lower C content (lower than 0.06% in these experiments), the scanning map and EPMA analysis of P show that P does not segregate significantly when the P content is less than 0.1wt%; and when the P content is high enough, P shows center segregation in both twin-roll cast strips and droplet samples. The negative segregation of P at the centre of the cast strips in thickness for high-P and high-C steels is observed. The P segregation mode is affected by the length of the mushy zone and the solidification outgrowth.

(5) The distributions of alloying elements in 0.2m drop tube samples are similar to those in 50m drop tube samples. The distributions of P and C are more uniform in FM samples than those in TM samples.

(6) In TM samples with high C, negative segregation of carbon is observed in high-C droplet samples, more C is distributed near the surface than that at the center, and more pearlites appear near the surface. The segregation of C is thought to relate to the solid solubility of alloying elements in different phases and the diffusibility of C during the solidification and recalescence process.

(7) The distribution of C and P is more uniform in B-bearing droplet samples than that of B-free ones for both TM and FM samples, which indicate that B atoms promote the uniformity of other alloying elements such as C and P.

(8) The micro-hardness of both twin-roll cast strips and droplet samples are significantly higher than those of the bulk solidified samples. Both C and P show strong solution strengthening, especially under rapid solidification conditions. With an increase in P content, the micro-hardness, strength and corrosion-resistance are improved with a sacrifice of plasticity. The micro-hardness of B-bearing samples is higher than those of B-free samples, while this tendency weakens when the volume of droplet samples increased.

(9) During the strip casting process, P is redistributed in the melting pool under the stress of liquid flow and squeezing of the rolls, and more P-rich melt prefer to distributed near the meniscus, which can enter the solidified skull under the rapid solidification condition and lead to the higher solute content at solidification front, and finally form the higher content of P near the surfaces than at the centre of the strip.

Acknowledgements

This work is financially supported by the Major State Basic Research Development Program of China (No.2004CB619108), the National Natural Science Foundation of China (Project No. 51074210), and the open fund of Key Laboratory of Materials Forming and Microstructure Properties Control, Liaoning Province (No. USTLKL2012-01).

Author details

Na Li[1*], Shuang Zhang[1], Jun Qiao[1], Lulu Zhai[1], Qian Xu[1], Junwei Zhang[1], Shengli Li[1], Zhenyu Liu[2], Xianghua Liu[2] and Guodong Wang[2]

*Address all correspondence to: huatsing2006@yahoo.com.cn

1 School of materials and metallurgy, University of Science and Technology Liaoning, Anshan, China

2 The State Key Laboratory of Rolling and Automation, Northeast University, Shenyang, China

References

[1] Hirata, K., Umezawa, O., & Nagai, K. (2002). Microstructure of cast strip in 0.1mass% C steels containing phosphorus [J]. *Materials Transaction*, 43(3), 305-310.

[2] Misawa, T., Kyuno, T., Suetaka, W., & Shimodaria, S. (1971). The mechanism of atmospheric rusting and the effect of Cu and P on the rust formation of low alloy steels [J]. *Corrosion Science*, 11(1), 35-48.

[3] Chen, Y. Y., Tzeng, H. J., Wei, L. I., & Shih, H. C. (2005). Mechanical properties and corrosion resistance of low-alloy steels in atmospheric conditions containing chloride [J]. *Materials Science and Engineering A*, 398(1-2), 47-59.

[4] Yoshida, N., Umezawa, O., & Nagai, K. (2004). Analysis on refinement of columnar γ grain by phosphorus in continuously cast 0.1 mass% carbon steel [J]. *ISIJ Int.*, 44(3), 547-555.

[5] Yoshida, N., Umezawa, O., & Nagai, K. (2003). Influence of phosphorus on solidification structure in continuously cast 0.1% carbon steel [J]. *ISIJ Int.*, 43(3), 348-357.

[6] Li, N., Liu, Z. Y., Lin, Z. S., Qiu, Y. Q., Liu, X. H., & Wang, G. D. (2006). Solidification structure of low carbon steels strips with different phosphorus contents produced by strip casting [J]. *Journal of Materials Science and Technology*, 22(6), 755-758.

[7] Emoto, K., Nozaki, T., & Yanazawa, T. (1986). Restructuring Steel Plant for Nineties [M]. *The Institute of Metals*, London, 151-160.

[8] Maruyama, T., Matsuura, K., Kudoh, M., & Itoh, Y. (1999). Peritectic Transformation and Austenite Grain Formation for Hyper-peritectic Carbon Steel [J]. *Tetsu-to-Hagané*, 85(8), 585-591.

[9] Maruyama, T., Kudoh, M., & Itoh, Y. (2000). Effects of Carbon and Ferrite-stabilizing Elements on Austenite Grain Formation for Hypo-peritectic Carbon Steel [J]. *Tetsu-to-Hagané*, 86(2), 86-91.

[10] Tavares, R. P. (1997). Vertical twin-roll caster:metal-mould heat transfer, solidification and product characterization[D], Ph.D. Thesis, McGill University.

[11] Kubaschewski, O. (1982). IRON-Binary Phase Diagrams [M], Springer-Verlag, Berlin/ Heidelberg, and Verlag Staheisen mbH, Düsseldorf.

[12] Tekko-Vinran, (1981). Handbook of Iron and Steel [M], 3rd ED., (ISIJ, Maruzen, Tokyo), 93.

[13] Leslie, W. C. (1981). The Physical Metallurgy of Steels [M], McGraw-Hill, London.

[14] Shin, Y. K., Kang, T., Reynolds, T., & Wright, L. (1995). Development of twin-roll strip caster for sheet steels [J]. *Ironmaking and Steelmaking*, 22(1), 35-44.

[15] Zhou, G. P., Liu, Z. Y., Yu, S. C., Chen, J., Qiu, Y. Q., & Wang, G. D. (2011). Formation of Phosphorous Surface Inverse Segregation in Twin-Roll Cast Strips of Low-Carbon Steels [J]. *Journal of Iron and Steel Research International*, 18(2), 18-23.

[16] Zhu, H. Q., Tang, Y. J., Guo, S. R., Zhang, Z. Y., Zhu, Y. X., Hu, Z. Q., & Shi, C. X. (1994). Effects of P, Zr and B on microstructure and segregation of directionally solidified IN738 superalloy [J]. *Acta Metallurgica Sinica (in Chinese)*, 30(7), A312-320.

[17] Miao, Y. C. (2001). Numerical Simulation of Solidification of Twin-roll Strip Casting Process [D], Ph.D. Thesis, Northeastern University, Shenyang, China.

[18] Li, N., Liu, Z. Y., Zhou, G. P., Liu, X. H., & Wang, G. D. (2010). Effect of phosphorus on the microstructure and mechanical properties of strip cast carbon steel [J]. *International Journal of Minerals Metallurgy and Materials*, 17(4), 417-422.

[19] Ortrud, K. (1982). Iron-Binary Phase Diagrams, Springer-verlag, Berlin.

[20] Flemings, M. C. (1974). Solidification Processing [M], McGraw-Hill, New York.

[21] Wang, H. Y., Liu, R. P., et al. (2005). Morphologies of Fe-66.7at.%Si alloy solidified in a drop tube [J]. *Science in China Series G: Physics Mechanics & Astronomy*, 48(6), 658-666.

[22] Yiu, Wingchan. (1989). Finite element simulation of heat f low in continuous casting [J]. *Advances in Engineering Software*, 11(3), 128-135.

[23] Zeoli, N., Gu, S., & Kamnis, S. (2008). Numerical modelling of metal droplet cooling and solidification [J]. *International Journal of Heat and Mass Transfer*, 51, 4121-4131.

[24] Li, N., Zhang, J. W., & Zhai, L. L. (2011). Segregation of C and P in steel droplets solidified in drop tube [J]. *Journal of Iron and Steel Research International*, 18(1-1), 282-286.

[25] Li, N., Sha, M. H., Xu, Q., Zhang, S., & Li, S. L. (2012). Rapid Solidification of Steel Droplets with Different Carbon Content in Drop Tube [J]. *China Foundry*, 9(1), 20-23.

IntechOpen